Energy Conversion and Management 51 (2010) 71–80

Contents lists available at ScienceDirect

Energy Conversion and Management

journal homepage: www.elsevier.com/locate/enconman

Direct torque and flux regulation of synchronous reluctance motor drives based on input–output feedback linearization

H. Abootorabi Zarchi [a,*], Gh.R. Arab Markadeh [b], J. Soltani [a]

[a] Faculty of Electrical and Computer Engineering, Isfahan University of Technology, Isfahan, Iran
[b] Department of Engineering, Shahrekord University, Shahrekord, Iran

ARTICLE INFO

Article history:
Received 27 January 2009
Accepted 29 August 2009
Available online 1 October 2009

Keywords:
Synchronous reluctance motor
Nonlinear controller
Input–output feedback linearization
Iron losses
Direct flux
Torque control

ABSTRACT

In this paper, a nonlinear speed tracking controller is introduced for three-phase synchronous reluctance motor (SynRM) on the basis of input–output feedback linearization (IOFL), considering the different control strategies (maximum torque per Ampere, high efficiency and minimum KVA rating for the inverter) related to this motor. The proposed control approach is capable of decoupling control of stator flux and motor generated torque. The validity and effectiveness of the method is verified by simulation and experimental results.

1. Introduction

In recent years, the synchronous reluctance motor (SynRM) has received much attention for many applications due to its simple and rugged construction [1–3]. A SynRM is advantaged on induction motor by the absence of rotor copper losses, on brushless motors by inexpensive rotor structure, and on switched reluctance motor by a much lower torque ripple and low noise. Compared to Surface type Permanent Magnet Synchronous Motor (SPMSM), it is capable of high-speed operation and for use in high-temperature environments. From control point of view, a SynRM has some advantages such that it can be considered an alternative to induction motor in many applications, such as robotics, traction and low-cost drives. Also the SynRM is suitable for super high speed applications in machine tools and molecular pumps [4].

For high performance SynRM drive, it is desirable to achieve optimum operation at maximum torque per Ampere (MTPA), high efficiency and minimum KVA rating for the inverter [5–7]. Detailed discussions and analysis of the control of a SynRM is given in references [5,6]. The analysis is restricted to the ideal motor, in which saturation and iron losses are ignored. However, the control of the SynRM is highly affected by both magnetic saturation and presence of iron losses [7]. Accurate representation of saturation effects requires detailed knowledge of magnetic behavior in both rotor d and q axes along with cross-saturation at different operating conditions. Due to the high reluctance associated with q-axis, it may be sufficient to consider magnetic saturation in d-axis only. The iron loss is considered in the SynRM by adding a shunt resistor in both d and q equivalent circuits [8] and authors' paper have considered aspects of the different control schemes when the effects of saturation and iron losses are taken into account. In [9], the motor parameters are online estimated on the basis of recursive least square (RLS) method, only using the proposed mathematical method and motor measured currents and voltages. In [10], the iron losses resistance is obtained by no-load test and the magnetic saturation is considered through a lookup table which shows the variation of direct axis inductance versus direct axis current while the little effect of magnetic saturation on parameter L_q is ignored.

In the past two decades many papers have been published which discuss the direct torque control (DTC) of induction motors [11–13], but a few papers have been reported regarding the DTC for SynRMs [14–20]. Although the conventional DTC [14–19] has merits of simple structure and excellent dynamic performance, but it shows some drawbacks such as switching frequency variation and a high sampling frequency is needed for its digital implementation. As a result, the high torque and current ripples which may deteriorate the performance of the drive system are produced [21].

To overcome the above drawbacks, in the last two decades, some researchers have tried to propose some different DTC space

* Corresponding author.
E-mail addresses: abootorabi9@yahoo.com (H. Abootorabi Zarchi), arab-gh@eng.sku.ac.ir (Gh.R. Arab Markadeh), j1234sm@cc.iut.ac.ir (J. Soltani).

0196-8904/$ - see front matter © 2009 Elsevier Ltd. All rights reserved.
doi:10.1016/j.enconman.2009.08.031

vector modulation (SVM) techniques or to improve switching state patterns [19,20]. In [19] a model-based predictive DTC has been presented for SynRM with constant switching frequency and relative long sampling time. To get that, the control algorithm calculates one step in advance the switching instants of two possible active voltage space phasors that build the demanding torque. Next, the trajectory of the stator flux is predicted with these two pre-selected voltage space phasors and the optimum of them, which leads to the best trajectory of the stator flux at the end of the cycle, is applied to the machine. The model-based of [19] is difficult to implement in practice and needs a lot of computation time and storage. In addition in [19], no any conventional strategy related to SynRM has been implemented. The iron loss has been ignored in the method described in [19]. Compared to [19], in this paper we introduce a new DTC–SVM scheme for SynRM in which the iron loss resistance is taken into account and can be applied for any control strategy (maximum torque per Ampere (MTPA), high efficiency and minimum KVA rating for the inverter) related to SynRM. In [20], a nonlinear method capable of high dynamic torque regulation and efficiency optimization of SynRM has been described based on input–output feedback linearization (IOFL) DTC–SVM. In [20], the SynRM efficiency is optimized by using Lagrange's theorem. Then, the efficiency optimization criterion and the motor torque are chosen as output variables.

The main purpose of this paper is to continue the research work described in [20] for the following gains:

- To achieve the SynRM direct torque and stator flux control.
- To eliminate two PI controllers employed in [20].
- To implement of MTPA and minimum input motor KVA rating control strategies, besides of efficiency-optimized strategy experimented in [20].

According to the authors little knowledge and search, this is the first time that the direct stator flux and torque control of SynRM is discussed based on IOFL DTC–SVM. To confirm the validity of the presented approach, simulation and experiments are carried out.

2. SynRM model including iron losses

In the synchronously rotating reference frame, the d and q axes equivalent circuits for the SynRM, including iron losses, have been described in [20]. Note that the resistance R_i represents the iron losses connected in parallel to both rotational and transient back EMF. From the equivalent circuit, we obtain that the electromagnetic torque T_e is proportional to the vector product of flux linkages and currents and can be obtained as (1), where P denotes the number of poles, L_d and L_q represent d and q axes inductances, respectively. Since R_i supplies an additional current path to each axis equivalent circuit, the torque depends not on measured terminal current, i_d^s and i_q^s, but on i_d^T and i_q^T. Therefore, the terminal currents can longer directly govern the torque.

$$T_e = \frac{3}{2}\frac{P}{2}\cdot\left(\lambda_d\cdot i_q^T - \lambda_q\cdot i_d^T\right) = \frac{3}{2}\frac{P}{2}\left(\frac{1}{L_q}-\frac{1}{L_d}\right)\lambda_d\lambda_q = \frac{3}{2}\frac{P}{2}\cdot(L_d-L_q)\cdot i_d^T\cdot i_q^T = K_T i_d^T i_q^T \tag{1}$$

Relation between $\left(i_{dT}^e \text{ and } i_{qT}^e\right)$ and $\left(i_{ds}^e \text{ and } i_{qs}^e\right)$ can be obtained as

$$\begin{bmatrix} i_d^s \\ i_q^s \end{bmatrix} = \begin{bmatrix} \left(1+p\frac{L_d}{R_i}\right) & \frac{-W_e L_q}{R_i} \\ \frac{W_e L_d}{R_i} & \left(1+p\frac{L_q}{R_i}\right) \end{bmatrix}\begin{bmatrix} i_d^T \\ i_q^T \end{bmatrix} \tag{2}$$

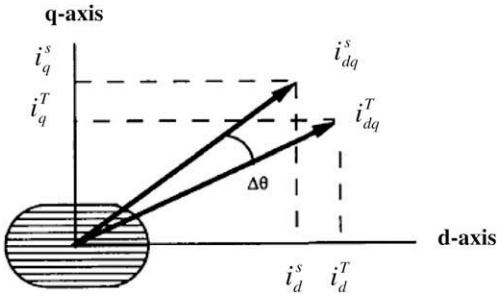

Fig. 1. The angle displacement between torque current (i_{dq}^T) and terminal current (i_{dq}^s) vectors.

Or

$$\begin{bmatrix} i_d^T \\ i_q^T \end{bmatrix} = \frac{R_i}{\left(p+\frac{R_i}{L_q}\right)\left(p+\frac{R_i}{L_d}\right)+W_e^2}\begin{bmatrix} \frac{1}{L_d}\left(p+\frac{R_i}{L_q}\right) & \frac{W_e}{L_d} \\ \frac{W_e}{L_q} & \frac{1}{L_q}\left(p+\frac{R_i}{L_d}\right) \end{bmatrix}\begin{bmatrix} i_d^s \\ i_q^s \end{bmatrix} \tag{3}$$

where $p=\frac{d}{dt}$. As shown in (3), the infinite R_i makes i_d^T and i_q^T identical to i_d^s and i_q^s, regardless of rotational speed ω_e. Having ignored R_i the optimal angle for maximum torque per Ampere is equal to 45° [6]. However, non negligible R_i produces the cross-coupling effects between the d and q circuits in (2), resulting in an additional angle shift between the torque current and terminal current vector as shown in Fig. 1 [7]. This misalignment brings out the steady-state torque error and makes the optimal angle of each strategy different from that of the infinite R_i case. Consequently, for high dynamic torque regulation and every strategy of SynRM when the iron losses are included, the compensation of the cross-coupling term is required and the voltage equations for SynRM should be expressed using the torque currents, rather than the terminal currents, as

$$v_d = R_s i_d^T + \Re L_d\frac{di_d^T}{dt} - \Re L_q W_e i_q^T \tag{4}$$

$$v_q = R_s i_q^T + \Re L_q\frac{di_q^T}{dt} + \Re L_d W_e i_d^T \tag{5}$$

where $\Re=\left(1+\frac{R_s}{R_i}\right)$. By assuming d and q axis fluxes as electrical states, (4) and (5) can be rewritten as

$$\dot{\lambda}_d = \frac{-R_s}{L_d\Re}\lambda_d + \omega_e\lambda_q + \frac{v_d}{\Re} \tag{6}$$

$$\dot{\lambda}_q = \frac{-R_s}{L_q\Re}\lambda_q - \omega_e\lambda_d + \frac{v_q}{\Re} \tag{7}$$

Choosing $\lambda_d = x_1, \lambda_q = x_2$ and $\omega_e = x_3$ as states and $v_d = u_1$, $v_q = u_2$ as inputs, the nonlinear dynamic model for the SynRM considering iron losses can be described in the following standard state-variable form:

$$\dot{X} = f(X) + g(X)U \tag{8}$$

where $X=[x_1 \quad x_2 \quad x_3]^T$, $U=[u_1 \quad u_2]^T$

$$f(X)=\begin{bmatrix} f_1 \\ f_2 \\ f_3 \end{bmatrix}=\begin{bmatrix} -\frac{R_s}{L_d\Re}x_1 + x_2x_3 \\ -\frac{R_s}{L_q\Re}x_2 - x_1x_3 \\ \left(\frac{3P}{4J_m}\left(\frac{1}{L_q}-\frac{1}{L_d}\right)x_1x_2 - \frac{T_l}{J_m}\right)/\frac{P}{2} - \frac{B_m\omega_e}{J_m} \end{bmatrix},$$

$$g(X)=[g_1 \quad g_2]=\begin{bmatrix} \frac{1}{\Re} & 0 \\ 0 & \frac{1}{\Re} \\ 0 & 0 \end{bmatrix} \tag{9}$$

where J_m is the rotor moment of inertia and B_m is the friction coefficient.

3. DTC-SVM of SynRM

According to the nonlinear model of SynRM, the linear control methods are not useful for wide range operation of SynRM. The Input–Output Feedback Linearization (IOFL) method is one of the nonlinear control methods that can be used to control of nonlinear plants such as SynRM.

Choosing the motor torque and the square of stator flux magnitude as output variables, output vector $y = [y_1 \quad y_2]^T$ can be defined as

$$\begin{aligned} y_1 &= T_e = \tfrac{3}{2}\tfrac{P}{2}\left(\tfrac{1}{L_q}-\tfrac{1}{L_d}\right)\lambda_d\lambda_q = \beta\lambda_d\lambda_q \\ y_2 &= |\lambda_s|^2 \end{aligned} \tag{10}$$

Taking the time derivatives of these outputs, gives

$$\begin{bmatrix}\dot{y}_1\\ \dot{y}_2\end{bmatrix} = \begin{bmatrix}L_f y_1\\ L_f y_2\end{bmatrix} + \begin{bmatrix}L_{g_1}y_1 & L_{g_2}y_1\\ L_{g_1}y_2 & L_{g_2}y_2\end{bmatrix}\begin{bmatrix}u_1\\ u_2\end{bmatrix} = \begin{bmatrix}L_f y_1\\ L_f y_2\end{bmatrix} + E(X)U \tag{11}$$

where $L_f y_i$, $i = 1, 2$, is the Lie derivative of y_i with respect to f. From (9), a first internal dynamic can be recognized and its stability will be proved later. $L_f y_i$ and $E(X)$ are given in the paper Appendix I. The matrix $E(X)$ is found to be nonsingular over all operating regions except null states.

Based on input–output feedback linearization the following control is introduced:

$$U = E^{-1}\begin{bmatrix}v_1 - L_f y_1\\ v_2 - L_f y_2\end{bmatrix} \tag{12}$$

Assuming the following state variables

$$\begin{aligned} \dot{y}_1 &= v_1 \\ \dot{y}_2 &= v_2 \end{aligned} \tag{13}$$

The system control efforts are defined by

$$\begin{aligned} v_1 &= -K_1 e_1 + \dot{T}_{ref} \\ v_2 &= -K_2 e_2 + |\dot{\lambda}_{sref}|^2 \end{aligned} \tag{14}$$

where K_1 and K_2 are positive constants and $e_1 = T_e - T_{eref}$ and $e_2 = |\lambda_s|^2 - |\lambda_{sref}|^2$. Subscript '*ref*' denotes the reference value.

In this paper, the nonlinear dynamics of the SynRM can be decomposed into an input–output part as (13) and an unobservable one by input–output linearization technique because total relative degree is not equal to the number of states. Since the stability of the whole SynRM dynamics is influenced not only by the input–output part, but also by the unobservable part, the behavior of the internal dynamics must be investigated. The corresponding internal dynamics of the SynRM in this paper can be given as (15), and the zero dynamics for checking the stability of internal dynamics is given as (16), where all outputs are maintained at zero. Although the zero dynamics are marginally stable as (16), the actual dynamics are supposed to be asymptotically stable due to the mechanical losses and viscosity damping [10]. Therefore, the whole system is said to be asymptotically minimum phase, because the zero dynamics of the SynRM system is stable.

$$\dot{x}_3 = \left(\frac{3P}{4J_m}\left(\frac{1}{L_q}-\frac{1}{L_d}\right)\lambda_{ds}\lambda_{qs} - \frac{T_l}{J_m}\right)\Big/\frac{P}{2} - \frac{B_m x_3}{J_m} \tag{15}$$

$$\dot{x}_3 = \left(-\frac{T_l}{J_m}\right)\Big/\frac{P}{2} - \frac{B_m x_3}{J_m} \tag{16}$$

4. SynRM control strategies

In this paper, the three well-known control strategies relating to SynRM (MTPA, efficiency-optimized and minimum KVA rating for the inverter) are considered under the constraint of constant torque production. In MTPA strategy, the minimization of SynRM stator current, in efficiency-optimized scheme, the minimization of input active power and in minimum KVA, the minimization of SynRM input apparent power are selected as control objectives. Based on Lagrange's theorem, it can be easily found that each strategy is satisfied when the torque curve and control objective curve are tangent at a point.

4.1. MTPA control

The maximum torque per Ampere can be obtained by minimizing the expression for the stator current under the condition of constant torque production at a certain speed.

The square stator current I_s^2 of the SynRM can be calculated as

$$I_s^2 = i_d^{s^2} + i_q^{s^2} = \left(i_d^T + i_d^l\right)^2 + \left(i_q^T + i_q^l\right)^2 \tag{17}$$

where i_d^l and i_q^l are the currents responsible for iron losses, which can be calculated as

$$i_d^l = -\omega_e \frac{L_q}{R_i} i_q^T, \quad i_q^l = \omega_e \frac{L_d}{R_i} i_d^T \tag{18}$$

Thus, the stator current vector can be expressed as (19) using (17) and (18)

$$I_s^2 = i_d^{T^2} + i_q^{T^2} + \frac{1}{R_i^2}\left(L_d^2 i_d^{T^2} + L_q^2 i_q^{T^2}\right)\omega_e^2 + \frac{2}{R_i}(L_d - L_q) i_d^T i_q^T \omega_e \tag{19}$$

4.2. Efficiency-optimized control

The maximum efficiency method can be obtained by minimizing the expression for the power into the machine under the constraint of constant power output. The input power P_{in} of the SynRM is obtained as

$$P_{in} = \frac{3}{2}\left(v_d i_d^s + v_q i_q^s\right) \tag{20}$$

Using (2)–(7) in steady-state condition, P_{in} can be expressed as (21)

$$\begin{aligned} P_{in} = {} & R_s\left(i_d^{T^2} + i_q^{T^2}\right) + \frac{1}{R_i}\left(1 + \frac{R_s}{R_i}\right)\left(L_d^2 i_d^{T^2} + L_q^2 i_q^{T^2}\right)\omega_e^2 \\ & + \frac{2R_s}{R_i}(L_d - L_q) i_d^T i_q^T \omega_e \end{aligned} \tag{21}$$

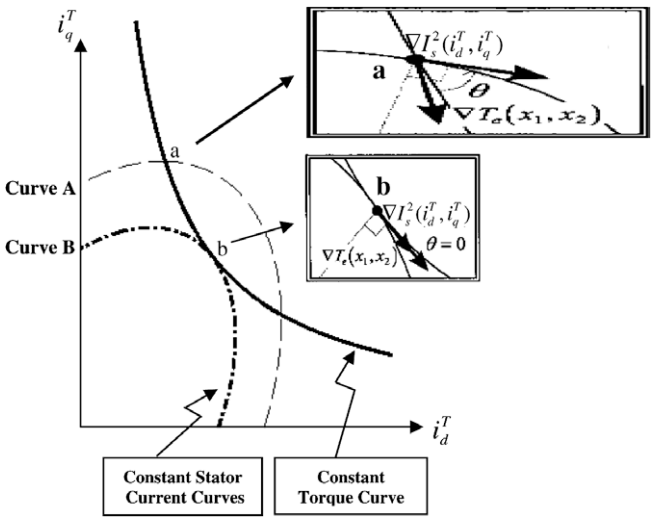

Fig. 2. Constant torque curve and stator current curve on i_d^T–i_q^T plane.

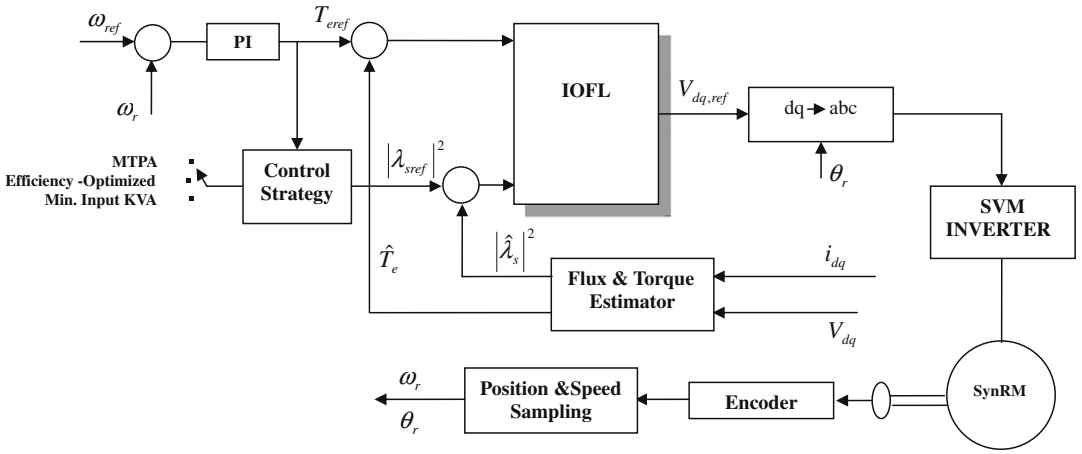

Fig. 3. Block diagram of SynRM drive system control.

4.3. Minimum input KVA control strategy

In order to obtain an expression for the minimum input KVA, one can minimize input apparent power S_{in} under the condition of constant power output. The input apparent power S_{in} of the SynRM is obtained as

$$S_{in}^2 = V_s^2 I_s^2 = \left(v_d^2 + v_q^2\right) I_s^2 \tag{22}$$

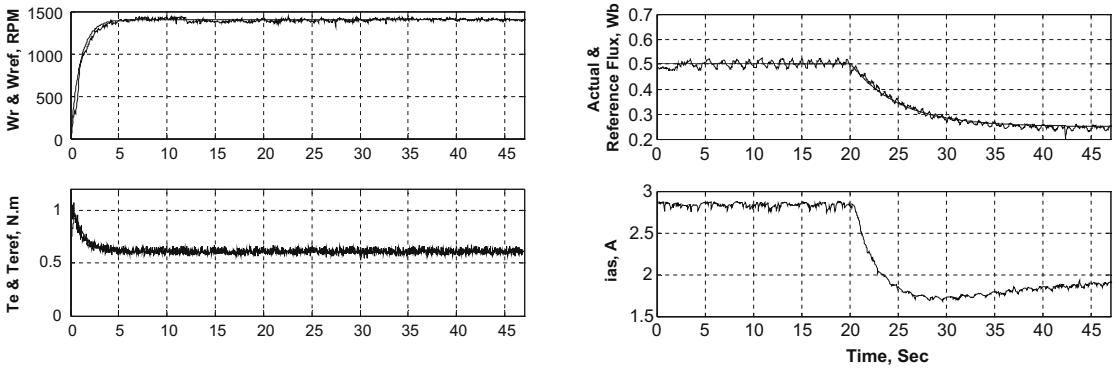

(a) Stator Flux Control

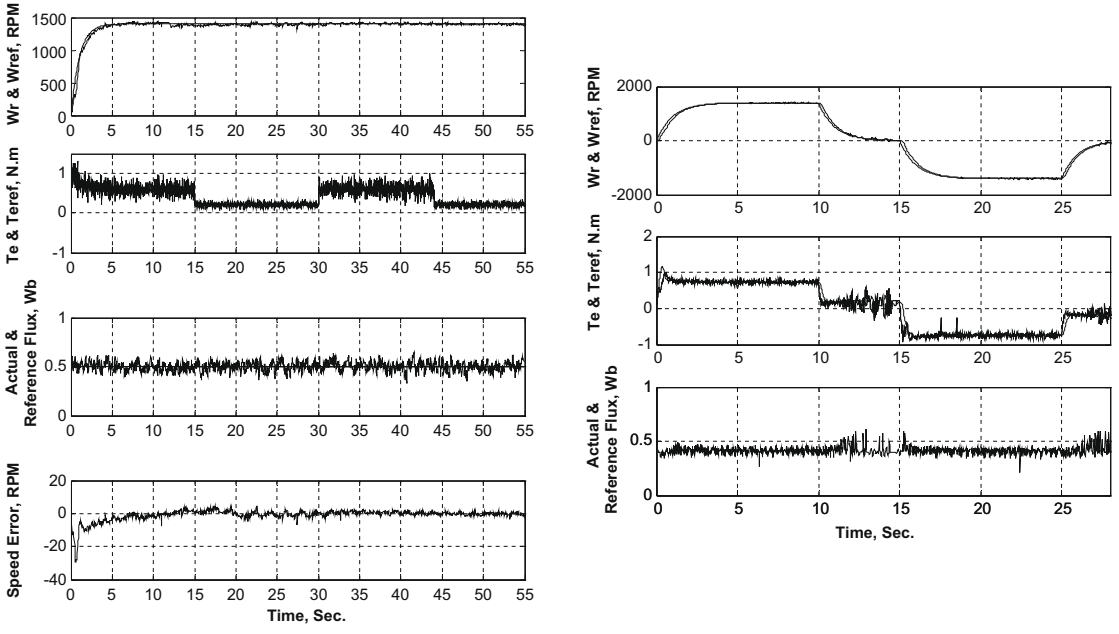

(b) Torque Control

Fig. 4. Simulation results.

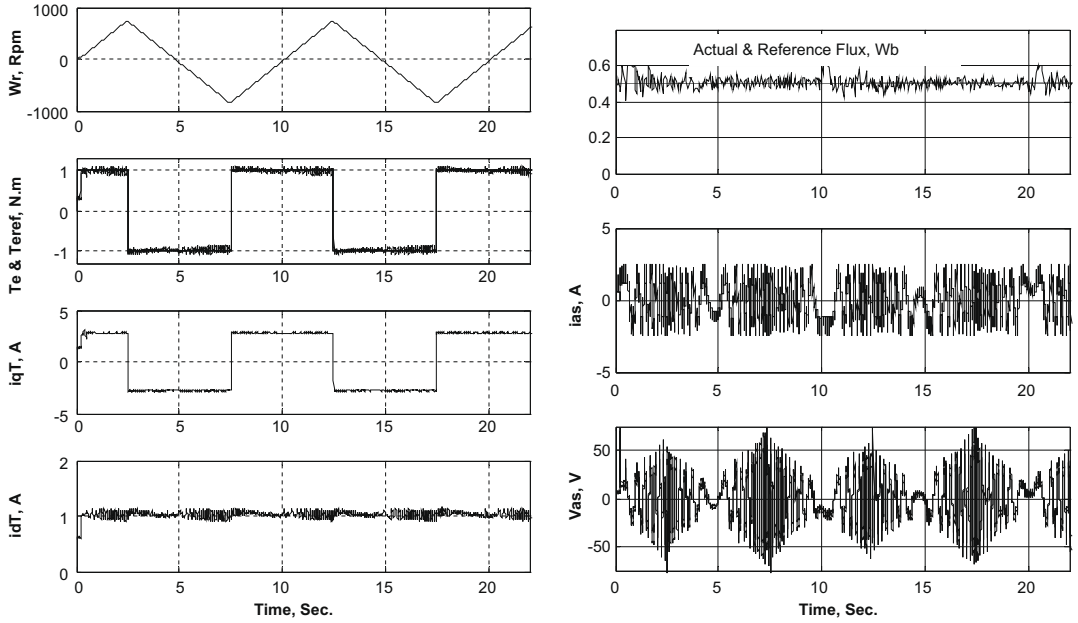

(c) Efficiency-Optimized Control Strategy

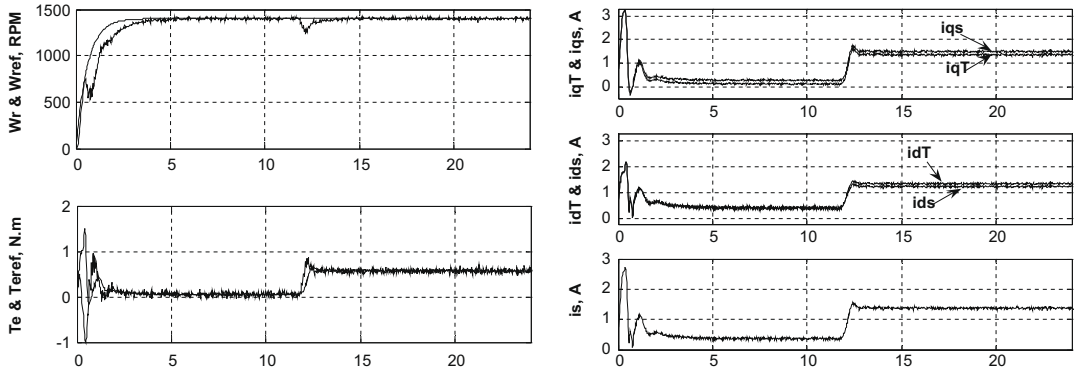

(d) MTPA Control Strategy

Fig. 4 (*continued*)

Using (2)–(5), and (19) in steady-state condition, S_{in} can be expressed as

$$S_{in}^2 = \frac{\omega_e^4}{R_i^2}\left(L_d^4 i_d^{T^4} + L_q^4 i_q^{T^4}\right) + \omega_e^2\left(L_d^2 i_d^{T^4} + L_q^2 i_q^{T^4}\right) + \frac{2\omega_e^3}{R_i}(L_d - L_q)\left(L_d^2 i_d^{T^3} i_q^T + L_q^2 i_d^T i_q^{T^3}\right) \quad (23)$$

In this paper, the minimization of Eqs. (19), (21) or (23) is regarded as one of the control objectives under the constraint of constant production. In Fig. 2, according to Eq. (1), the constant torque curve can be drawn as a hyperbola on the $i_d^T - i_q^T$ plane. On the same plane, at a speed, a curve representing every strategy, takes the form of an ellipse. Under the constraint of constant torque production, if an operating point is set at point "a" in Fig. 2, the curve A is supposed to be a control objective curve such as constant stator current curve. If an operating point is set at "b", the curve B is another control objective curve. Based on Lagrange's Theorem [20], it can be easily found that control objective is minimum when the torque curve and control objective curve are tangent at a point if and only if their gradient vectors are parallel. This means that $\nabla T_e\left(i_d^T, i_q^T\right)$ must be a scalar multiple of $\nabla\left(I_s^2, P_{in} \text{ or } S_{in}\right)$ at the point of tangency (see "b" in Fig. 2), so that

$$\|\nabla T_e\left(i_d^T, i_q^T\right)\|\|\nabla I_s^2(i_d^T, i_q^T)\| \sin\theta = 0 \quad \text{in MTPA} \quad (24)$$

$$\|\nabla T_e\left(i_d^T, i_q^T\right)\|\|\nabla P_{in}(i_d^T, i_q^T)\| \sin\theta = 0 \quad \text{in efficiency-optimized control} \quad (25)$$

$$\|\nabla T_e\left(i_d^T, i_q^T\right)\|\|\nabla S_{in}(i_d^T, i_q^T)\| \sin\theta = 0 \quad \text{in min. KVA} \quad (26)$$

where θ is the angle between $\nabla T_e\left(i_d^T, i_q^T\right)$ and $\nabla\left(I_s^2, P_{in} \text{ or } S_{in}\right)$.

4.4. MTPA strategy

$$\|\nabla T_e(i_d^T, i_q^T)\|\|\nabla I_s^2(i_d^T, i_q^T)\| \sin\theta = 2K_T\left[\left(1 + \frac{L_q^2}{R_i^2}\omega_e^2\right) i_q^{T^2} - \left(1 + \frac{L_d^2}{R_i^2}\omega_e^2\right) i_d^{T^2}\right] = 0 \Rightarrow i_q^T = \pm i_d^T \cdot \sqrt{\frac{\left(1 + \frac{L_d^2}{R_i^2}\omega_e^2\right)}{\left(1 + \frac{L_q^2}{R_i^2}\omega_e^2\right)}} \quad (27)$$

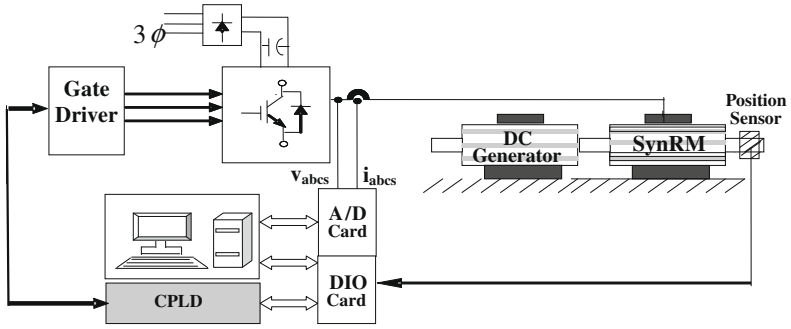

(a) Laboratory Implementation Block Diagram

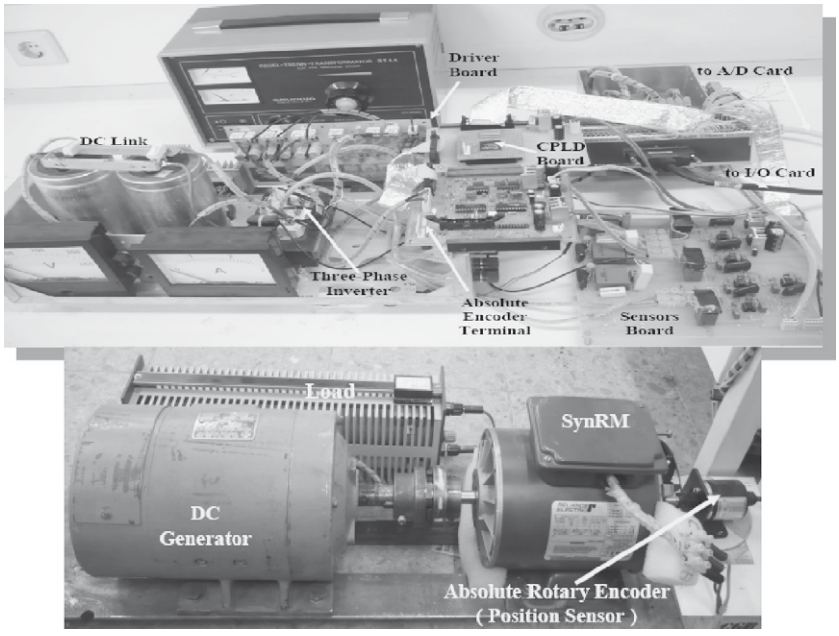

(b) SynRM Drive System Hardware

Fig. 5. Experimental setup.

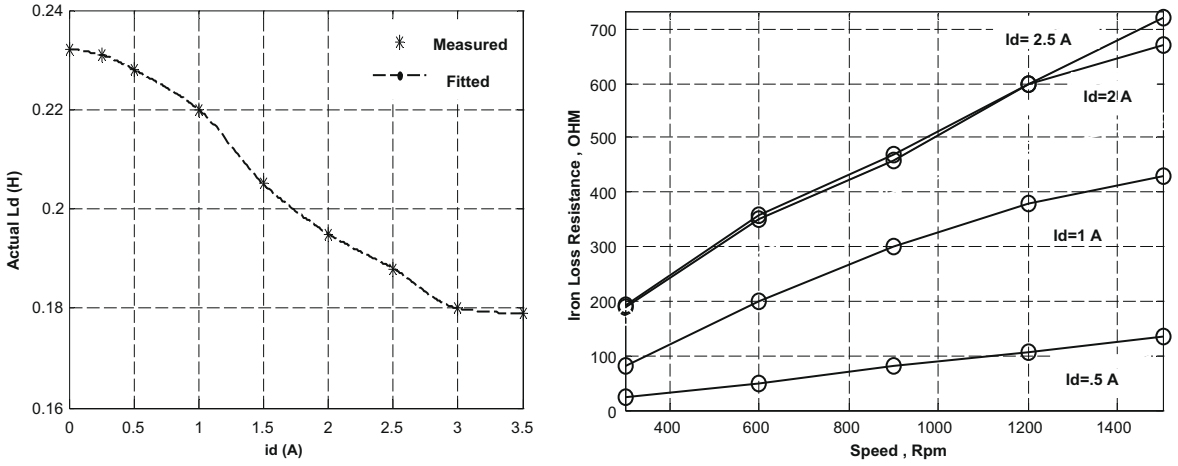

(a) Variation of d-axis inductance L_d with d-axis current i_d

(b) Measured Iron Loss Resistance R_i

Fig. 6. Parameter variations: (a) *d*-axis inductance L_d with *d*-axis current i_d and (b) iron loss resistance R_i.

4.5. Efficiency-optimized control strategy

$$||\nabla T_e(i_d^T, i_q^T)||||\nabla P_{in}(i_d^T, i_q^T)|| \sin\theta = 3K_T\left[\left(R_s + \frac{1}{R_i}\left(1+\frac{R_s}{R_i}\right)L_d^2\omega_e^2\right)i_q^{T^2} - \left(R_s + \frac{1}{R_i}\left(1+\frac{R_s}{R_i}\right)L_q^2\omega_e^2\right)i_d^{T^2}\right] = 0 \Rightarrow i_q^T = \pm i_d^T \cdot \sqrt{\frac{\left(R_s + \frac{1}{R_i}\left(1+\frac{R_s}{R_i}\right)L_q^2\omega_e^2\right)}{\left(R_s + \frac{1}{R_i}\left(1+\frac{R_s}{R_i}\right)L_d^2\omega_e^2\right)}} \quad (28)$$

4.6. Min. KVA strategy

$$||\nabla T_e\left(i_d^T, i_q^T\right)||||\nabla S_{in}\left(i_d^T, i_q^T\right)|| \sin\theta = 0 \Rightarrow \frac{\omega_e^2}{R_i^2}\left(L_q^4 i_q^{T^4} - L_d^4 i_d^{T^4}\right) + \left(L_q^2 i_q^{T^4} - L_d^2 i_d^{T^4}\right) + \frac{\omega_e}{R_i}(L_d - L_q)\left\{L_q^2 i_q^{T^3} i_d^{T^4} - L_d^2 i_d^{T^3} i_q^{T^4}\right\} = 0 \quad (29)$$

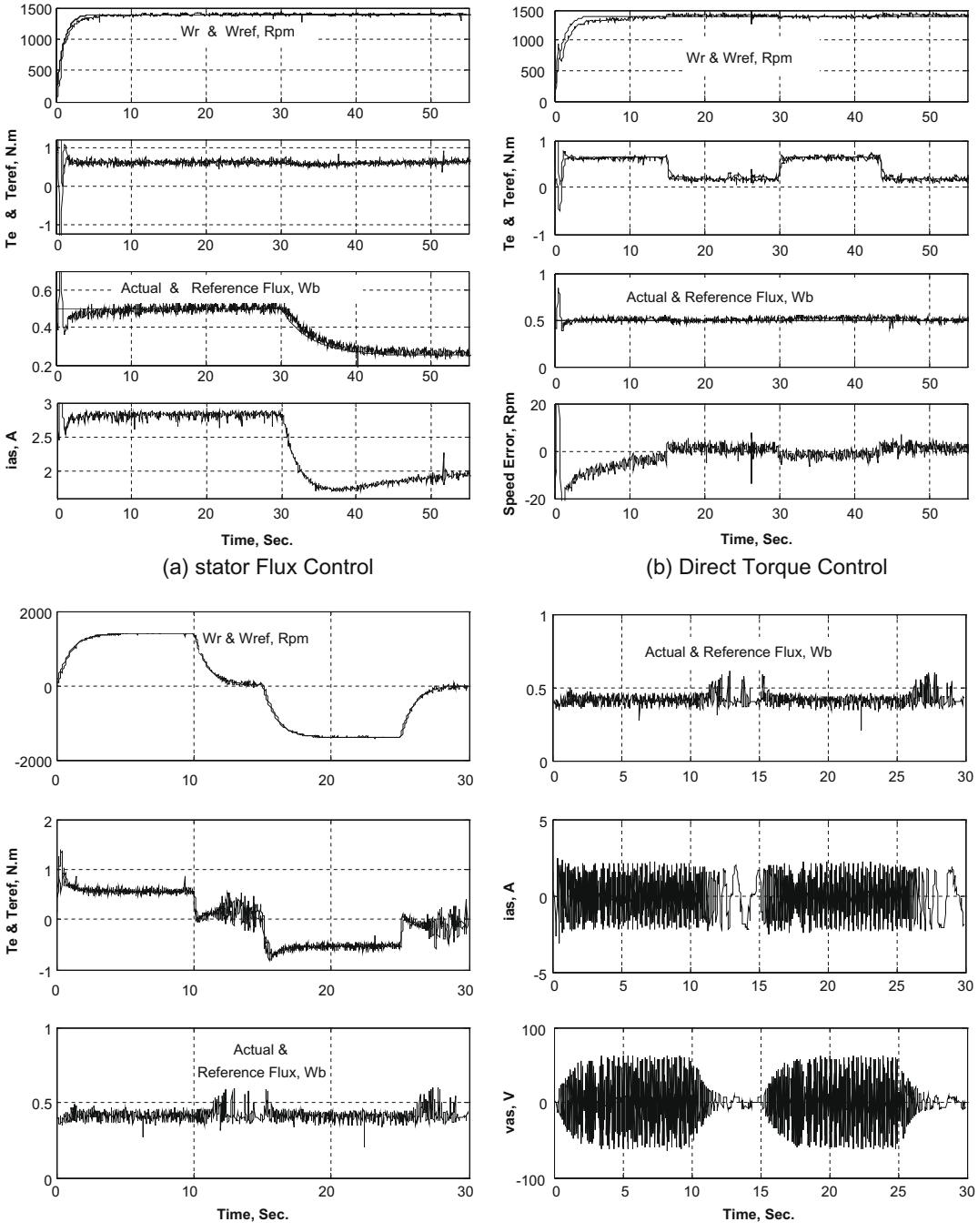

(a) stator Flux Control

(b) Direct Torque Control

(c) Direct Torque Control (with a Two-directional Speed Reference Signal)

Fig. 7. Experimental results (Decoupled Stator Flux and Torque Control of SynRM).

5. Simulation results

Overall block diagram of the drive system control is shown in Fig. 3. Based on IOFL the motor supply voltage is synthesized from stator d and q axis voltage commands $\left(v_d^*, v_q^*\right)$, using a two level space vector modulation SVM-based PWM inverter. A C^{++} step by step computer program was developed to model the drive system control of Fig. 3. In this program, the system dynamic equations are solved by a static Range–Kutta fourth order method. In our proposed control approach the system controller gains are obtained

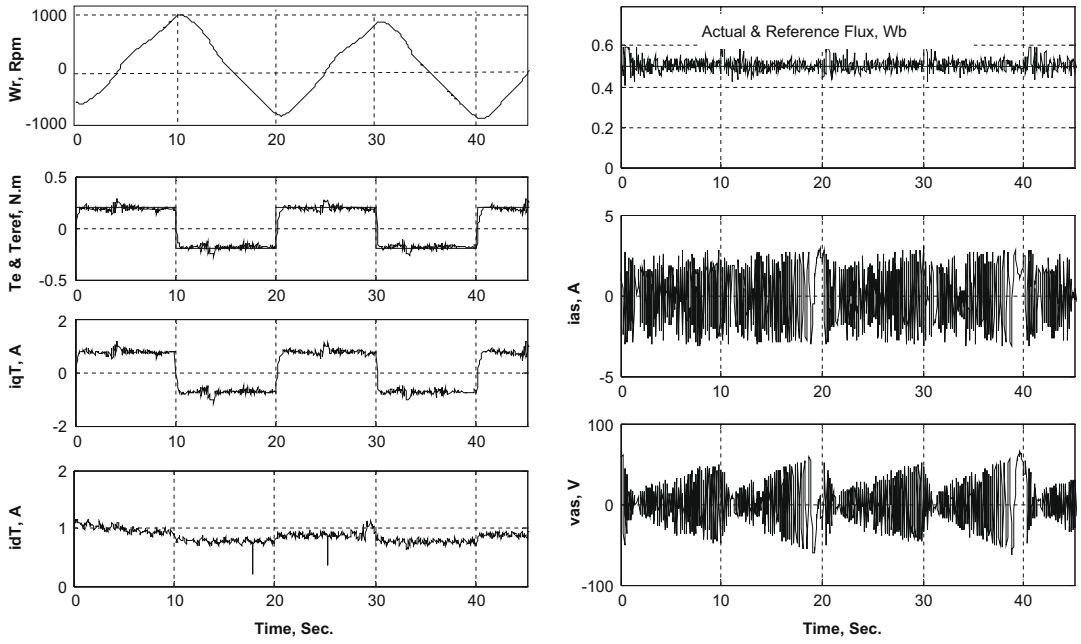

(a) Efficiency-Optimized Control Strategy

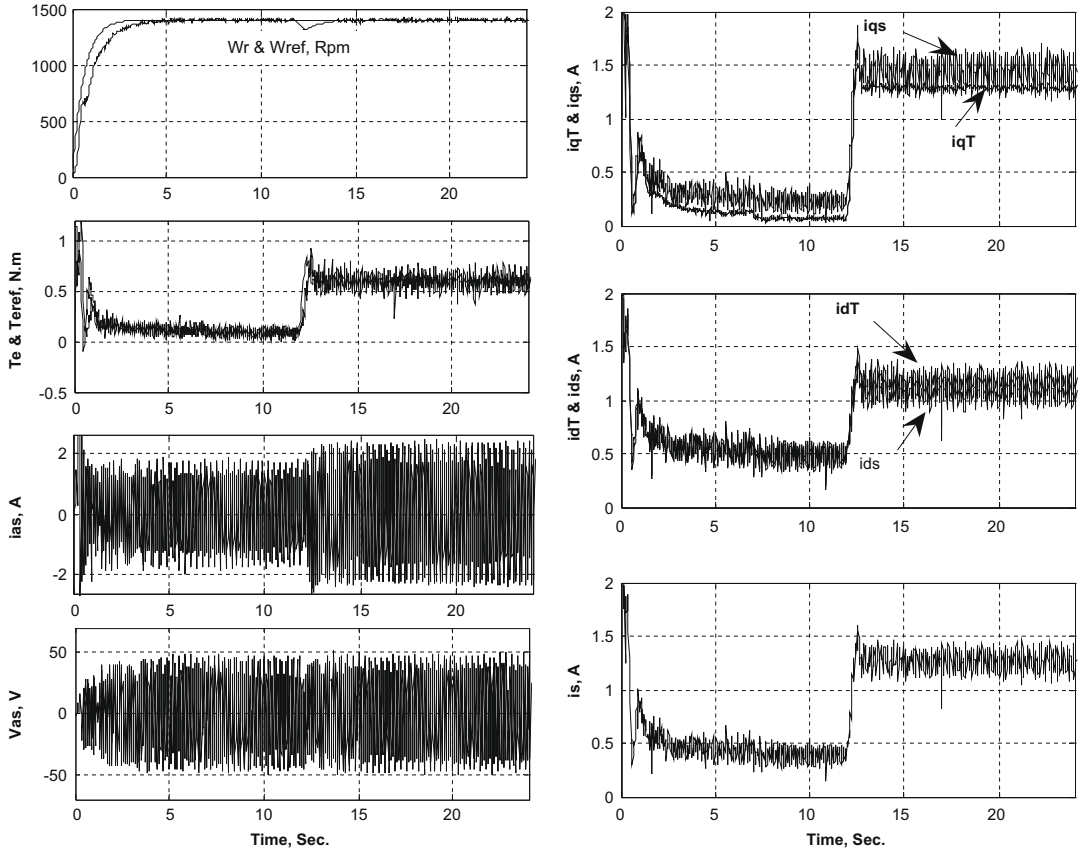

(b) MTPA Control Strategy

Fig. 8. Experimental results: (a) efficiency-optimized control strategy and (b) MTPA control strategy.

by trial and error method which are given by $K_p = 0.3$, $K_i = 0.05$ and $K_1 = K_2 = 225$. The specifications and parameters of three-phase SynRM used in our simulation program are given in Appendix II. Simulation results obtained for SynRM direct stator flux and torque control are shown in Fig. 4a and b. From these results one can see that for a chosen stator flux and torque reference signals, the SynRM rotor speed is properly tracked. Considering MTPA and efficiency-optimized control strategies relating to SynRM, the simulated results are presented in Fig. 4c and d. As shown in figures, the torque and flux references are well regulated to the respective commands and the internal states $\left(i_d^T, i_q^T\right)$ move to the optimal point along the demanded torque curves. The speed W_e increases and decreases rather linearly which means that the produced torque is regulated well to its desired value by the help of the proposed nonlinear controller.

6. Experimental setup and results

6.1. Experimental system setup

For practical evaluation of the actual system performance, a PC-based prototype system was built and tested. The experimental setup corresponding to overall system block diagram shown in Fig. 3 is depicted in Fig. 5 and consists of the following sections.

A 0.37 kW three-phase SynRM and a 1.1 kW DC generator as its load; Three-phase voltage source inverter and its isolation board; Voltage and current sensors board; 96 bit Advantech digital Input–Output card; 32-channel Advantech A/D converter card; CPLD board and a personal computer (PC) for calculating required signals and viewing the registered waveforms. The 0.37 kW SynRM parameters are reported in Appendix II.

The SynRM is supplied by a three-phase inverter with a symmetrical two level space vector modulation. A Xilinx XC95288xl CPLD has been selected for real time implementation of switching patterns using a switching frequency of 5 kHz.

The CPLD board communicates with PC via the digital Advantech PCI-1753 I/O board. CPLD in experimental setup realizes the following tasks: Switching pattern generation of IGBT switches based on SVM technique, providing a useful dead time in the so-called switching patterns of power switches, generation of the synchronizing signal for data transmission between PC and hardware and shutting down the inverter in the case of emergency conditions such as over current or PC hanging states. The inverter has been designed & implemented specifically for this experiment using SKM75 GD 124 D SEMIKRON module.

The required drive board has been designed by hcpL 316 J which is fast and intelligent IGBT driver and guarantees a reliable isolation between the high voltage and control boards. The DC link voltage and stator phase currents and voltages are measured by Hall-type LEM sensors. All measured electrical signals are filtered using the separate analogue second order low pass filters with 1.5 kHz bandwidth which is enough higher than our operating frequency and then converted to digital signals using an A/D card with 10 μs conversion time. The rotor position is measured in respect to axis of stator "A" phase using an AUTONICS absolute encoder with 1024 pulses per round. The output pulse of position sensor is sent to the PC via I/O card.

6.2. Experimental results

Using the same conditions adopted to get SynRM simulation results as described in previous section, the experimental results were obtained as shown in Figs. 7 and 8. The motor d-axis inductance L_d versus i_d has been obtained from a practical test, considering Fig. 6a. The iron loss resistance R_i can be acquired by measuring the input power under no-load condition and the measured results has been plotted in Fig. 6b. Since R_i varies with operating frequency and magnetizing current, this value is updated to the controller in real time according to the load condition and speed.

Experimental results obtained for SynRM direct stator flux and torque control are shown in Fig. 7. From these results one can see that for a chosen stator flux and torque reference signals, the SynRM rotor speed is properly tracked. Considering Efficiency-Optimized control and MTPA strategies relating to SynRM, the simulated results are presented in Fig. 8a and b, respectively. A close agreement can be seen between simulation and practical results and a Little disagreement seen between these two set of results can be described by inaccuracies that exist in our data acquisition system, SVPWM voltage source inverter effects and the dead times of inverter switching signals.

Table I
Specifications and parameters of three-phase SynRM for simulations and experiments.

P_n = 370 W	V_n = 230	I_n = 2.8 A
$L_{md,unSat}$ = 232 mH	$L_{md,Sat}$ = 178 mH	L_{mqn} = 118 mH
R_{sn} = 2.95 Ω	f_n = 60 Hz	*No.of poles* = 4
T_{en} = 1.9 Nm	J_m = .015 Kg m^2	B_m = .003 Nm/rad/s

7. Conclusion

In this paper, at the first, the SynRM direct stator flux and torque control has been discussed using input–output feedback linearization. In addition, based on proposed control approach, the control strategies of MTPA, optimized-efficiency and minimum input KVA related to SynRM have been adapted. A close agreement can be seen between simulation and practical results and a Little disagreement seen between these two set of results may be because of inaccuracies that exist in our data acquisition system, SVPWM voltage source inverter effects and the dead times of inverter switching signals.

Appendix I

$$L_f y_1 = -\beta\left(\frac{R_s}{\Re}\lambda_d\lambda_q\left(\frac{1}{L_d}+\frac{1}{L_q}\right)+\omega_e(\lambda_d^2-\lambda_q^2)\right) \tag{A1}$$

$$L_f y_2 = -\frac{R_s}{\Re}\left(\frac{\lambda_d^2}{L_d}+\frac{\lambda_q^2}{L_q}\right) \tag{A2}$$

$$E(X) = \begin{bmatrix} \beta\lambda_q & \beta\lambda_d \\ 2\lambda_d & 2\lambda_q \end{bmatrix} \tag{A3}$$

Appendix II

See Table I.

References

[1] Lipo TA. Synchronous reluctance machines-a viable alternative for AC drives? Electr Mach Power Syst 1991;19:659–71.
[2] Consoli A, Russo F, Scarcella G, Testa A. Low and zero-speed sensorless control of synchronous reluctance motors. IEEE Trans Indus Appl 1999;35(5):1050–7.
[3] Boldea I, Muntean N, Nasser SA. Robust low cost implementation of vector control of reluctance synchronous machines. IEEE Proc Electr Power Appl 1994;141(I):1–6.
[4] Chiba A, Fukao T. A closed-loop operation of super high-speed reluctance motor for quick torque response. IEEE Trans Indus Appl 1992;28(3):600–6.
[5] Betz RE, Lagerquist R, Jovanovic M, Miller TJE, Middleton RH. Control of synchronous reluctance machines. IEEE Trans Indus Appl 1993;29(6):1110–22.
[6] Matsuo T, Lipo TA. Field oriented of synchronous reluctance machine (SynRM). IEEE 1993;IA-33:1146–53.

[7] Xu L, Xu X, Lipo TA, Novotry DW. Vector control of a synchronous reluctance motor including saturation and iron loss. IEEE Trans Indus Appl 1991;27(5):977–85.
[8] Betz RE. Theoretical aspects of the control of synchronous reluctance machines. IEEE Proc B 1992;139(4).
[9] Ichikawa S, Tomita M, Doki S, Okuma S. Sensorless control of synchronous reluctance motors based on extended EMF models considering magnetic saturation with online parameter identification. IEEE Trans Indus Appl 2006;42(5):1264–74.
[10] Rashad EM, Radwan TS, Rahman MA. A maximum torque per ampere vector control strategy for synchronous reluctance motors considering saturation and iron losses. IEEE IAS 2004:2411–7.
[11] Rodriguez J, Pontt J, Silva C, Huerta R, Miranda H. Simple direct torque control of induction machine using space vector modulation. Electron Lett 2004;40(7):412–3.
[12] Lascu C, Boldea I, Blaabjerg F. Direct torque control of sensorless induction motors: a sliding mode approach. IEEE Trans Indus Appl 2004;40(2):582–90.
[13] Arab GR, Soltani J. Robust direct torque control of adjustable speed sensorless induction machine drive based on space vector modulation using a pi predictive controller. Springer; 2006. p. 485–96.
[14] Consoli A, Cavallars C, Scarcella G, Testa A. Sensorless torque control of synchronous motor drives. IEEE Trans Power Electron 2000;15(1):28–35.
[15] Liu TH, Hsu HH. Adaptive controller design for a synchronous reluctance motor drive system with direct torque control. IET Electr Power Appl 2007;1(5):815–24.
[16] Zhou LQ, Direct torque control of ALA synchronous reluctance machines based on modified integrator. In: IEEE PCC'07, 2–5 April 2007. p. 271–4.
[17] Dong J, Zhengming Z, Yao D, Wei G. Position sensorless direct torque control os synchronous reluctance with permanent magnet motor. In: CES/IEEE 5th IPEMC'06, 14–16 August 2006. p. 1–5.
[18] Zhou LQ, Zhu JH, Gu CL. A direct torque control of ALA synchronous reluctance machine and its DSP-based implementation. In: IECON'05, 31st annual conference of IEEE, November 2005. p. 1689–94.
[19] Morales Caporal R, Pacas M. A predictive torque control for the synchronous reluctance machine taking into account the magnetic cross saturation. IEEE Trans Indus Electron 2007;54(2).
[20] Lee HD, Kang SJ, Sul SK. Efficiency-optimized direct torque control of synchronous reluctance motor using feedback linearization. IEEE Trans Indus Electron 1999;46(1):192–8.
[21] Casadei D, Profumo F, Serra G, Tani A. FOC and DTC: two viable schemes for induction motors torque control. IEEE Trans Power Electron 2002;17(5): 779–87.

	Mark	Rank	Abbreviated Journal Title	ISSN	JCR Data						EigenfactorTM Metrics		JCR©2009 Impact Factor Regenerated by Jones			
					Total Cites	Impact Factor	5-Year Impact Factor	Immediacy Index	Articles	Cited Half-life	Eigenfactor™ Score	Article Influence™ Score				
5		1	4OR-Q J OPER RES	1619-4500	130	0.75		0	31	4.2	0.00125					
6		2	AAPG BULL	0149-1423	7204	1.448	2.548	0.522	69	>10.0	0.00666	0.858				
2229		2225	ENERG CONVERS MANAGE	0196-8904	6791	1.944	2.465	0.209	383	5.6	0.01938	0.642				
2230		2226	ENERG EXPLOR EXPLOIT	0144-5987	169	0.491	0.715	0.407	27	4.6	0.00035	0.116				
2231		2227	ENERG FUEL	0887-0624	9498	2.319	2.594	0.331	826	4.9	0.02493	0.58				
2232		2228	ENERG J	0195-6574	1077	1.857	2.186	0.279	43	8.3	0.00528	1.272				

باسمه تعالی

تاریخ:۱۴۰۱/۳/۲۳

فرم خود ارزیابی مقاله ژورنالی

(توسط متقاضی)

همکار ارجمند

با توجه به اهمیت داوری صحیح مقاله ها، خواهشمند است به پرسش های زیر با دقت پاسخ دهید. همچنین، گزارش طرح های پژوهشی، پایان نامه کارشناسی ارشد و رساله دکتری خود را به ضمیمه مدارک تسلیم دارید. درخواست می شود لطفا به همپوشانی آثار، توجه ویژه ای مبذول فرمایید.

شماره ردیف: 3 **عنوان مقاله: (با 49 ارجاع)**

Direct torque and flux regulation of synchronous reluctance motor drives based on input–output feedback linearization

۱- آیا مقاله ای با محتوای مشابه در جای دیگری چاپ شده است؟ خیر ■ آری☐ نمی دانم☐

۲- آیا این مقاله با مقاله های دیگر شما همپوشانی دارد؟ (*به مانند: روش حل، نتایج و ...*) خیر ■ آری☐ درصد همپوشانی:

شماره ردیف مقاله: عنوان مقاله‌ای که همپوشانی دارد:

۳- درجه علمی مجله علمی پژوهشی معتبر (JCR , Scopus – علمی پژوهشی داخلی) که مقاله در آن منتشر شده است:

عالی■ بسیار خوب☐ خوب☐ متوسط☐ ضعیف☐

٤- محتوای مقاله از نظر ویژگی های زیر چگونه است؟

۱-اعتبار علمی: عالی■ خوب☐ متوسط☐ ضعیف☐

۲- نوآوری و ابتکار: عالی■ خوب☐ متوسط☐ ضعیف☐

۵- آیا مقاله مستخرج از پایان نامه‌ی کارشناسی ارشد و یا از رساله‌ی دکترای جنابعالی می باشد؟

خیر ☐ آری■ درصد همپوشانی:80%

در صورتی که پاسخ به سؤال بالا مثبت باشد، به پرسش های زیر پاسخ فرمایید:

الف- فرض های به کار رفته و محتویات اصلی تا چه حد بر موارد همانند در پایان نامه و یا رساله منطبق است؟

ب- آیا روش تحلیل و یا نتیجه گیری با موارد همانند در پایان نامه و یا رساله مشابهت دارد؟

٦- آیا این مقاله با مقالات کنفرانسی شما همپوشانی دارد؟

خیر■ آری☐ میزان درصد همپوشانی:

شماره ردیف مقاله: عنوان مقاله‌ای که همپوشانی دارد:

۷- آیا این مقاله با طرح های پژوهشی یا طرح اینترنشیپ شما همپوشانی دارد؟ خیر■ آری☐ درصد همپوشانی:

عنوان طرح:

۸- آیا مقاله (برای استادی شما) با مقالات دانشیاری شما همپوشانی دارد ؟ خیر■ آری☐ درصد همپوشانی:

عنوان مقاله‌ای که همپوشانی دارد:

لطفاً چنانچه نظر اصلاحی یا تکمیلی دارید در این صفحه یا در پشت برگه درج فرمایید.

حسین ابوترابی زارچی

امضاء